The effects of the aerodynamic interaction on the performance of two Flettner rotors

Bordogna, G.; Muggiasca, S.; Giappino, S.; Belloli, M.; Keuning, J. A.; Huijsmans, R. H.M.

DOI
10.1016/j.jweia.2019.104024

Publication date
2020

Document Version
Final published version

Published in
Journal of Wind Engineering and Industrial Aerodynamics

Journal of Wind Engineering & Industrial Aerodynamics 196 (2020) 104024

Contents lists available at ScienceDirect

Journal of Wind Engineering & Industrial Aerodynamics

journal homepage: www.elsevier.com/locate/jweia

The effects of the aerodynamic interaction on the performance of two Flettner rotors

G. Bordogna [a,*], S. Muggiasca [b], S. Giappino [b], M. Belloli [b], J.A. Keuning [a], R.H.M. Huijsmans [a]

[a] Section of Ship Hydromechanics, Delft University of Technology, Mekelweg 2, 2628 CD, Delft, the Netherlands
[b] Department of Mechanical Engineering, Politecnico di Milano, Via La Masa 1, 20156, Milan, Italy

ARTICLE INFO

Keywords:
Flettner rotor
Rotating cylinder
Aerodynamic interaction
Rotor sail
Magnus effect
Wind assisted ship propulsion

ABSTRACT

Flettner rotors are nowadays becoming a widespread solution for wind-assisted propulsion. To increase the fuel savings of the ship on which they are installed, multiple devices are typically used. However, in the performance estimate of these hybrid ships, it is currently assumed that Flettner rotors operate independently, regardless of the number of devices employed and their relative position on the ship's deck. The present investigation deals with a wind-tunnel experimental campaign aimed at understanding the aerodynamic interaction effects on the performance of two similar Flettner rotors. The study indicates that the aerodynamic performance of the two Flettner rotors is affected by their interaction, and, generally, this is most noticeable when the devices are set closer to each other and when they are aligned with the wind direction. It is demonstrated that, depending on the apparent wind direction, the layout of the Flettner rotors on the ship's deck has a remarked influence on the driving and heeling force coefficients of the entire rig. Lastly, the velocity ratio is found to play a key role in the determination of how the interaction affects the Flettner rotor aerodynamic performance.

1. Introduction

In the context of wind-assisted propulsion, Flettner rotors are currently attracting increasing interest as a viable technology to reduce the fuel consumption of commercial ships. The Flettner rotor is a rotating cylinder that generates an aerodynamic lift due to the Magnus effect, and it owes its name to German engineer Anton Flettner, who first introduced it in 1925 (Flettner, 1925). The physical phenomena associated with Flettner rotors and, more broadly, to rotating cylinders, were studied quite extensively over the past years. As a result of these research efforts, it was possible to identify the influence of several parameters, as for example the velocity ratio, the endplate size, the aspect ratio and the Reynolds number, on the aerodynamic performance of a single Flettner rotor. However, to increase the fuel-saving potential of the designated vessel, in real-life applications, multiple Flettner rotors are often used (see Fig. 1). The use of multiple Flettner rotors in a confined space as it is the deck of a ship is likely to lead to a change in performance of each of the installed device due to their aerodynamic interaction.

Although it is tenable that, in general, this situation would be the norm, this phenomenon is nowadays largely neglected. In fact, the aerodynamic thrust generated by a set of Flettner rotors is now commonly calculated as the simple arithmetic sum of the thrust produced by each of the installed devices, i.e. the aerodynamic interaction effects are fully disregarded (Li et al., 2012; Traut et al., 2012, 2014; Pearson, 2014; De Marco et al., 2016). On the other hand, in other cases in which the interaction effects are taken into account, an arbitrary reduction in aerodynamic force is assumed. Eggers (2016), for example, assigns a reduction in lift force to the leeward Flettner rotor when the ship is sailing in certain conditions in which the aerodynamic interaction effects are assumed to be most relevant.

The reason for these simplifications in modelling the aerodynamic thrust generated by a set of Flettner rotors is because, substantially, the literature lacks publications on this topic. This is also remarked by De Marco et al. (2016) and Badalamenti (2010). There are, in fact, numerous publications on the phenomena associated with arrangements of two or more steady cylinders, whereas considerably fewer studies focused on sets of rotating cylinders. As it will be argued herewith, in either case, the literature currently available is of limited practical use for real-life Flettner rotor applications.

Due to its importance in many engineering fields, the problem of interference between two or more steady cylinders in tandem, staggered or side-by-side arrangement, was largely studied during the years. Comprehensive summaries on this topic can be found in the works of Zdravkovich (2003), Sumner (2010) and in ESDU (2012), in which details on the forces and pressures of each cylinder are provided together

* Corresponding author.
E-mail address: g.bordogna@tudelft.nl (G. Bordogna).

https://doi.org/10.1016/j.jweia.2019.104024
Received 17 May 2019; Received in revised form 11 September 2019; Accepted 27 October 2019
Available online 11 November 2019

Nomenclature

AR	Aspect ratioH/D
AWA	Apparent Wind Angle
C_D	Drag coefficient, $F_D/(0.5 \cdot \rho \cdot V^2 \cdot H \cdot D)$
C_L	Lift coefficient, $F_L/(0.5 \cdot \rho \cdot V^2 \cdot H \cdot D)$
C_X	Driving force coefficient, $F_X/(0.5 \cdot \rho \cdot V^2 \cdot H \cdot D)$
C_Y	Heeling force coefficient, $F_Y/(0.5 \cdot \rho \cdot V^2 \cdot H \cdot D)$
D	Cylinder diameter
D_E	Endplate diameter
F_L, F_D	Lift and drag force
F_X, F_Y	Driving and heeling force
H	Cylinder span
k	Velocity ratio, U_{tan}/V
Re	Reynolds number, $(V \cdot D)/\nu$
U_{tan}	Cylinder tangential velocity
V	Incoming flow velocity
WA	Wind angle in experiments on two Flettner rotors
ν	Kinematic viscosity of air
ρ	Density of air

with extensive analyses of the flow pattern. The same research topic attracted considerable attention also for problems related to wake-induced vibrations. See, for example, the studies of Bearman (2011), Assi et al. (2010) and Diana et al. (2014), in which cases, the focus is on the dynamic response of the analysed structures. Although the current research shares the aim of studies on multiple steady cylinders, i.e. how two or more cylinders interfere depending on their relative position, the forces and flow patterns generated by rotating cylinders are not comparable to those of steady cylinders. The findings relative to steady cylinders have, therefore, limited utility in the context of the present work.

Regarding studies on multiple rotating cylinders, considerable fewer publications can be found in the literature. Prandtl (1926), joint with his extensive research on the single Flettner rotor, provided flow visualizations of two side-by-side counterrotating cylinders. Unluckily, no results regarding the interaction effects on the aerodynamic forces were reported. The research efforts of Ueda et al. (2003) and Watson (1995) deal with analytical solutions for two rotating cylinders in Stokes flows. In particular, Ueda et al. (2003), provide the drag coefficients for several velocity ratios and spacings between cylinders. For the same type of flow, Garzon and Figueroa (2017) analytically calculated the velocity field generated by an array of four rotating cylinders. The results for four different rotation sets are compared with PIV measurements and show good agreement. Sungnul and Moshkin (2009), Yoon et al. (2009) and Fallah et al. (2011) conducted numerical studies on two counter-rotating cylinders in side-by-side and staggered arrangement. The computations were carried out in laminar flow, i.e. $Re < 100$, and the effects of the velocity ratios and the cylinders' relative positions on the lift and drag coefficients were computed. The studies agree in indicating that both the cylinders' relative positions and velocity ratios strongly influence their lift and drag coefficients. On the other hand, the work of Guo et al. (2009) comprised a series of PIV measurements for Reynolds numbers ranging between $425 < Re < 1130$ and for velocity ratios $0 \leq k \leq 4$. The cylinders were set in a side-by-side arrangement and, also in this case, they were counter rotating. The study does not include any result regarding the effects of the aerodynamic interference on the cylinders' lift and drag coefficients. However, in line with Sungnul and Moshkin (2009), Yoon et al. (2009) and Fallah et al. (2011), the authors conclude that the spacing and the cylinders' velocity ratios are important parameters to determine the flow pattern. This is supported by the finding that the vortex shedding of the cylinders is suppressed as the velocity ratio increases.

A similar investigation was conducted by Kumar et al. (2011). In their research, in fact, the authors study the flow around two side-by-side counter rotating circular cylinders to investigate through PIV visualizations the vortex suppression mechanism. The investigation was carried out at Reynolds numbers varying from $Re = 100$ to $Re = 500$, velocity ratios in the range $0 \leq k \leq 5$ and several transversal distances between the two cylinders.

The characteristics of the numerical and experimental investigations carried out until today on multiple rotating cylinders limit the applicability of the available literature to the present work. In fact, the research efforts here discussed were typically conducted in the laminar or creeping flow regime as well as using counter-rotating cylinders. A part to the flow regime that, for the scope of this research it is a limit on its own, to generate positive thrust Flettner rotors typically spin in the same direction.

In this scenario, the present study aims to be the first attempt in

Fig. 1. The E-ship 1 is a wind-assisted ship equipped with four Flettner rotors.

investigating the effects of the interaction on the aerodynamic performance of multiple Flettner rotors. The experimental campaign comprised two distinct series of experiments: first, tests on a single Flettner rotor were carried out in order to establish a baseline for comparison. For these experiments, measurements of the velocity field were also taken at several locations in the wake of the single Flettner rotor. At a later time, two analogous Flettner rotors were tested for a range of different relative positions and velocity ratios. In this series of tests, their lift and drag coefficients were measured and then compared to those of the single Flettner rotor to investigate the effects of the aerodynamic interaction. These results were eventually used to study the performance, expressed in terms of driving and heeling force coefficients, of different Flettner rotor layouts when installed on the deck of a ship.

The present investigation, together with a previous study of the authors regarding the effect of the Reynolds number on a Flettner rotor's aerodynamic coefficients (Bordogna et al., 2019), aims at gaining a better understating of the real-life performance of these devices when used on a ship for wind-assisted propulsion.

2. Experimental setup

2.1. Wind tunnel and flow characteristics

The experiments were carried out in the boundary-layer test section of Politecnico di Milano wind tunnel. The test section is 13.84 m wide, 3.84 m high and 35 m long (Fig. 2). Due to the large dimensions, the wind-tunnel chamber has a rather large standard turbulence intensity, i.e. $I_u = 2\%$. The choice of a boundary-layer test section (a value of $I_u = 2\%$ is common for this type of facilities) was due to the size of the Flettner rotors employed in the tests. No studies were conducted on the influence of the turbulence intensity on the results. Nonetheless, it should be pointed out that, in real-life applications, Flettner rotors are likely to experience a flow with turbulence intensity $I_u > 2\%$. In this respect, it appears that a facility with a large turbulence intensity better represents the conditions in which full-scale Flettner rotors operate rather than a test section with a lower I_u. The boundary layer thickness of the wind-tunnel chamber is about 0.2 m. Considering the wind-tunnel boundary layer and the height of the Flettner rotor bottom static endplate from the ground (see Fig. 3), it can be assumed that the Flettner rotors experienced a straight wind profile throughout the experimental campaign.

The flow velocity, used to calculate all the aerodynamic coefficients, was measured with the wind-tunnel pitot tube that is hung at a distance of 1.2 m from the ceiling (Fig. 2). All tests were conducted at a wind speed of $V = 5$ m/s, leading to a Reynolds number

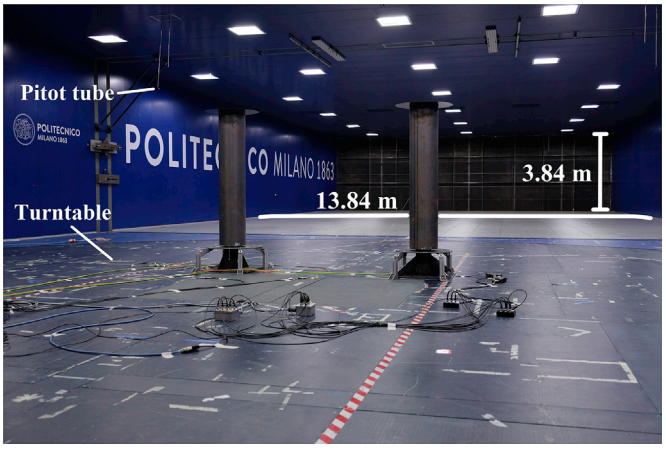

Fig. 2. The two Flettner rotors in the boundary layer test section of Politecnico di Milano wind tunnel.

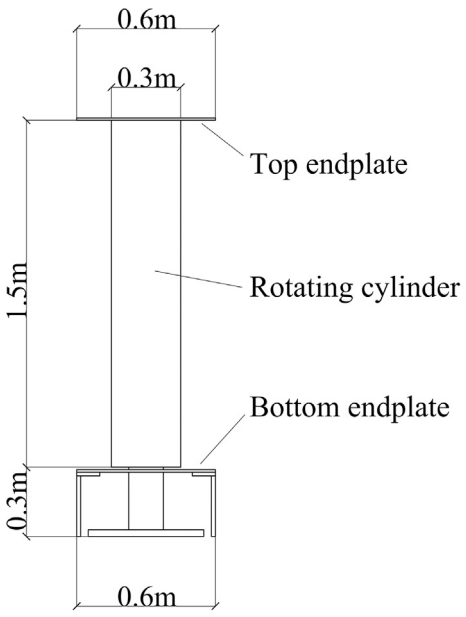

Fig. 3. Main dimensions of the Flettner rotors used in the experiments.

$Re = 1.0 \cdot 10^5$. Nonetheless, some tests were carried out at lower and higher Reynolds numbers. In fact, some experiments on the single Flettner rotor were conducted at a wind speed $V = 3.5$ m/s ($Re = 7.0 \cdot 10^4$), $V = 10$ m/s ($Re = 1.8 \cdot 10^5$) and $V = 12.5$ m/s ($Re = 2.4 \cdot 10^5$). No corrections were made due to blockage effects as the blockage ratio was less than 1%.

2.2. The Flettner rotor

The Flettner rotor type used throughout the experimental campaign had a diameter $D = 0.3$ m, a span $H = 1.5$ m and an aspect ratio $AR = 5$. Two endplates, of diameter $D_E/D = 2$, were used. The top endplate rotated with the cylinder while the bottom endplate was fixed at a height of 0.3 m from the ground (Fig. 3).

The aspect ratio and the size of the endplates used in the current experiments are comparable to those commonly used for wind-assisted propulsion. In particular, in respect to the endplate size, Badalamenti and Prince (2008) demonstrated that, for $D_E/D \geq 2$, the endplate size has a negligible influence on C_L and a moderate influence on C_D up to velocity ratio $k = 2$ (that is the highest velocity ratio investigated in the current work). The same publication also indicates that using endplates larger that $D_E/D = 2$ produces a steep increase of the power consumption necessary to rotate the cylinder. Given these conditions, an endplate size $D_E/D = 2$ appears to be a good comprise and, in fact, is the endplate size typically used for Flettner rotor applications.

The rotating cylinder comprised three different main parts: a hollow square section beam welded to a steel ground plate, an aluminium static cylinder and a thin steel rotating cylinder on top of which the carbon fibre endplate was attached. The electric engine used to spin the cylinder was hung on a plate secured to the top of the static cylinder. The rotation was passed to the external cylinder by means of a flexible joint that connected the engine shaft with the top plate shaft, to which the external rotating cylinder was bolted (Fig. 4).

The two cylinders used in the experiments were analogous except for the measurement instruments employed. In fact, one cylinder was equipped with two ATI Mini 45 F/T balances, that are 6-axis sensors, while the other with three HBM Z6FD1 load cells, that are monodirectional sensors. The internal arrangement of the two cylinders, specifically the connection between the hollow beam and the static cylinder, had to be modified to fit the different measurement instruments used. This is shown in Fig. 4.

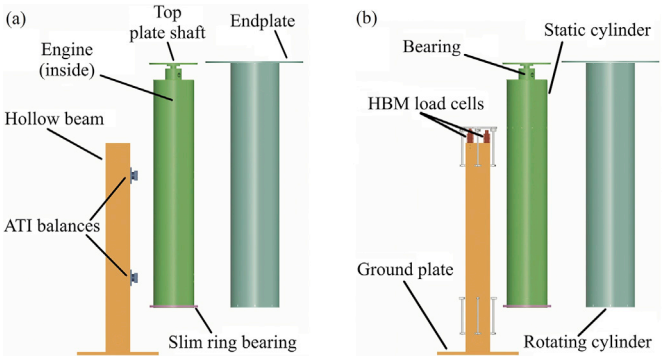

Fig. 4. Flettner rotor components with ATI balances (a) and HBM load cells (b).

2.3. Single Flettner rotor setup

During the experiments, the single Flettner rotor was positioned in the centre of the wind-tunnel turntable and the lift and drag forces were measured for all velocity ratios considered. The velocity ratio k is defined as the ratio between the cylinder tangential velocity and the incoming flow velocity:

$$k = U_{tan}/V \tag{1}$$

For velocity ratios $k = 0$, $k = 1$, $k = 1.5$ and $k = 2$, moreover, measurements of the velocity field were taken at several positions in the wake of the rotating cylinder.

Four Cobra Probes were used to measure the velocity field. The Cobra Probe is a multi-hole pressure probe capable to measure the three velocity components within an angle range of ±45° at a frequency of 2000 Hz. The Cobra Probes were mounted on a vertical bar at four different heights, namely 0.47 m (Cobra 4), 0.85 m (Cobra 3), 1.24 m (Cobra 2) and 1.62 m (Cobra 1) from the ground (Fig. 5). Measurements of the velocity field were taken at four longitudinal distances downstream the Flettner rotor, corresponding to 1.5, 3, 7.5 and 15 diameters. At each longitudinal position, the vertical bar was automatically displaced from -1.5 m to +1.5 m with respect to the cylinder centreline in steps of 0.15 m.

For this series of tests, the Flettner rotor equipped with the ATI balances was used.

2.4. Two Flettner rotor setup

The two Flettner rotors were tested for three different spacings, defined as the longitudinal distance from the cylinders' vertical axes of symmetry (see Fig. 6), corresponding to 3, 7.5 and 15 diameters. For each spacing, the wind-tunnel turntable was rotated at various angles between 15° and 180° in order to change the cylinders' relative position with respect to the incoming wind direction.

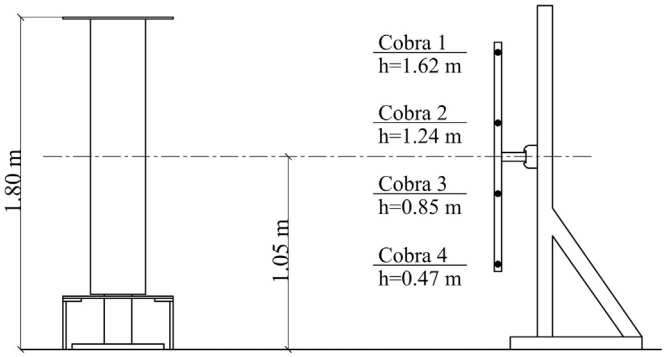

Fig. 5. Vertical position of the Cobra Probes with respect to the Flettner rotor.

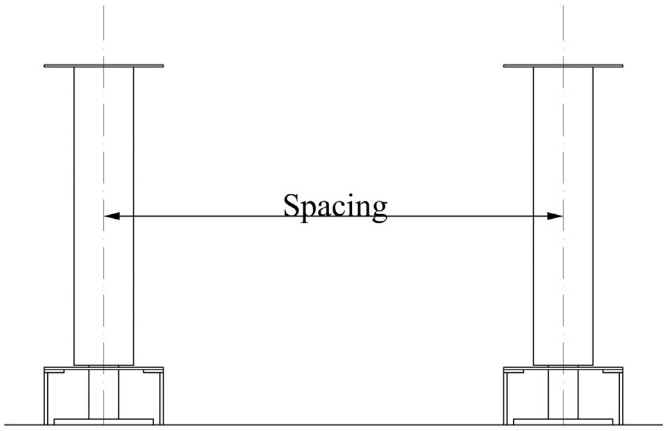

Fig. 6. Definition of spacing between two Flettner rotors.

For each case, the Flettner rotors were spun for all combinations of velocity ratios generated by $k = 1$, $k = 1.5$ and $k = 2$, leading to a matrix of nine velocity ratios. Throughout the experiments, the cylinders rotated clockwise and the lift and drag forces of Flettner rotor A and Flettner rotor B were measured following the conventions depicted in Fig. 7.

2.5. Measurement uncertainty

The uncertainty of the experimental study was calculated according to the ISO "Guide to the Expression of Uncertainty in Measurement" (ISO/IEC 98-3, 2008). The expanded uncertainty with 95% confidence level, u_{95}, was calculated from the standard uncertainty related to the measurement precision, u_{pr}, and the standard uncertainty of the bias errors of the measurement instruments, u_{bias}. During the experiments, repetitions were carried out exclusively for $k = 1$, $k = 1.5$ and $k = 2$, and for Reynolds number $Re = 1.0 \cdot 10^5$. The measurement uncertainties were therefore calculated for these conditions. The standard uncertainty related to the measurement precision reads:

$$u_{pr} = \sqrt{(\sigma^2/N)} \tag{2}$$

where σ is the standard deviation of the N considered data points.

On the other hand, the standard uncertainty related to the bias errors of the measurement instrument is the sensitivity of the measurement instrument accuracy, obtained by means of calibration tests, respect to the quantity of interest. u_{bias} can then be calculated by taking the partial derivative of the instrument accuracy with respect to the quantity to be analysed. The value of u_{bias} differ for the ATI balance and the HBM load cell. The expanded uncertainty with 95% confidence level is thus

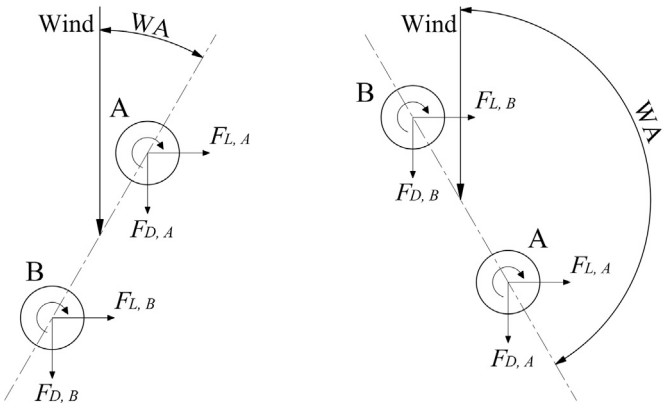

Fig. 7. Conventions used for the two-Flettner rotor experiments for wind angles $WA < 90°$ (left) and wind angles $WA > 90°$ (right).

calculated according to:

$$u_{95} = c \cdot \sqrt{\left(u_{pr}^2 + u_{bias}^2\right)} \quad (3)$$

where the coverage factor c is set to $c = 2$.

Regarding the tests on the two Flettner rotors, it should be pointed out that repetitions were not carried out for the entire set of spacings and flow angles analysed. In fact, for each considered velocity ratio, the tests were repeated only for one spacing and one flow angle. The assumption is that the measurement uncertainties calculated for those conditions can also be applied to all other comparable conditions, i.e. same velocity ratio but different spacing and different flow angle. This is justifiable because the measurement precision error appears to be marginal compared to the bias error of the measurement instrument. This is particularly the case for the HBM load cells, for which the bias error appears to be considerably large. The reason of a large bias error is due to the fact that the measurement instruments chose for the current experiments had to have a sufficiently large load range along the vertical axis to withstand the weight of the Flettner rotor but, consequently, the load ranges along the lift and drag axes resulted to be over-dimensioned. One possibility to reduce the measurement instrument bias error would have been to increase the wind speed at which the experiments were carried out. However, in the current experimental campaign, this was not feasible because, to reach the desired velocity ratios, the Flettner rotors should have spun at much higher rotational speeds, and this was a concern for the structural limits of the Flettner rotor assembly with respect to vibrations. In fact, it was decided to establish a safety limit of 11 Hz (the lowest eigenfrequency of the Flettner rotor assembly was 16 Hz), meaning that to reach velocity ratio $k = 2$ the highest achievable wind speed was $V = 5$ m/s.

The uncertainties derived with the method herewith described are included in the results in the form of error bars. For the sake of clarity, the error bars are given just for one data point for each setup (single and double Flettner rotor setup) and for each quantity of interest (C_L, C_D, C_X and C_Y). This is sufficient to understand the magnitude of the uncertainties with respect to the relative measurements because, as previously explained, the standard uncertainty related to the measurement precision u_{pr}, that depends on the different testing conditions (i.e. wind angle, spacing, velocity ratio), is negligible compared to u_{bias}. Moreover, regarding the driving and heeling force coefficients, for which the results are presented for the entire Flettner rotor rig, the measurement uncertainties were calculated as the summation in quadrature of u_{95} of Flettner rotor A and u_{95} of Flettner rotor B. The measurement uncertainties of the single Flettner rotor, on the other hand, are calculated for all considered conditions using u_{bias} relative to the ATI balance, since it was the measurement instrument employed in the single Flettner rotor experiments.

3. Results

3.1. Results of the single Flettner rotor

This section deals with the results of the experiments carried out on the single Flettner rotor. The aim of these tests was twofold: on one hand, the force measurements were necessary to create reference data for the comparison with the results of the double Flettner rotor tests whereas, on the other hand, the measurements of the velocity field provided a useful insight to understand the nature of the aerodynamic interaction effects. As already mentioned in Section 2.1, the tests were carried out at $Re = 10^5$, however, experiments at $Re = 7.0 \cdot 10^4$, at $Re = 1.8 \cdot 10^5$ and $Re = 2.4 \cdot 10^5$ (only steady cylinder) were also performed. In the former case, the reason was to better compare the results of the single Flettner rotor with the available literature data. In the latter case, the aim was to investigate, within the possibilities offered by the setup employed, whether a higher Reynolds number would affect the lift and drag coefficients in the same manner described in a previous publication of the authors (Bordogna et al., 2019) as well as to gather a better insight on the flow regime in which the experiments were carried out.

The direction of rotation and the reference system used during the single Flettner rotor experiments are depicted in Fig. 8.

In Fig. 9, the results of the single Flettner rotor are provided and compared with the results of Badalamenti and Prince (2008), who performed tests at Reynolds number $Re = 1.9 \cdot 10^4$ on a Flettner rotor of similar aspect ratio ($AR = 5.1$), and using a similar configuration (one rotating and one fixed endplate of $D_E/D = 2$). Although due to the setup used in the current work, it was unfeasible to reach such a low Reynolds number, the results of the current experiments obtained at $Re = 7.0 \cdot 10^4$ show an excellent agreement with the results of Badalamenti and Prince (2008).

On the other hand, the curves obtained at a higher Reynolds number (black and green curves) show the same trend due to scale effects reported in a previous study of the authors (Bordogna et al., 2019). In this publication, the interested reader can find further information regarding the influence of the Reynolds number on the Flettner rotor aerodynamic coefficients.

A series of tests on the steady Flettner rotor was also carried out to investigate the behaviour of the drag coefficient in relation to the flow regime (see Fig. 10).

The results of Fig. 10 indicate that at $Re = 1.0 \cdot 10^5$ the decrease of the drag coefficient does not yet occur, meaning that the experiments carried out at $Re = 1.0 \cdot 10^5$ were conducted in the subcritical flow regime. In this flow conditions, a value of the drag coefficient of $C_D = 0.85$ is in agreement with other investigations relative to three-dimensional circular cylinders with an endplate (Belloli et al., 2016).

The results of the velocity field measurements obtained at velocity ratios $k = 0, k = 1, k = 1.5$ and $k = 2$ are given in Fig. 11. For the sake of conciseness, only the results of Cobra probe 2 are reported. The results of Cobra probe 2 and Cobra probe 3, in fact, show a similar trend and they can be considered representative for most of the cylinder's span. Cobra probe 1 and Cobra probe 4, on the other hand, captured a more peculiar trend due to their position closer to the Flettner rotor top and bottom tip vortices (see Fig. 5). The results of Cobra probe 1 and Cobra probe 4 only affect a minor section of the Flettner rotor' span and, for this reason, are less useful to understand the relation between the measured velocity field and the Flettner rotor aerodynamic forces.

The results depicted in Fig. 11 illustrate the mean velocity magnitude and the mean direction of the flow. The velocity magnitude, that is normalized with the free stream velocity, is indicated by the colourmap and the vector size. Conversely, the direction of the flow is suggested by the vector orientation. The results are given in terms of longitudinal (x-axis) and transversal (y-axis) distance from the cylinder's vertical axis of symmetry, normalized with the cylinder diameter. The Flettner rotor rotates clockwise as shown in Fig. 8, and it is located at the centre of the reference system ($x/D = 0, y/D = 0$). As it can be appreciated from the results, the cylinder wake, that is clearly visible for $k = 0$, is reduced with the increase of the velocity ratio. At $k = 1$, the wake is already strongly

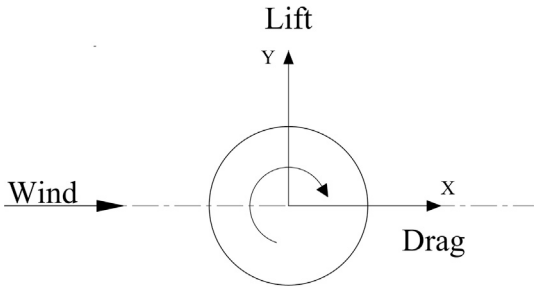

Fig. 8. Direction of rotation and reference system used for the single Flettner rotor tests.

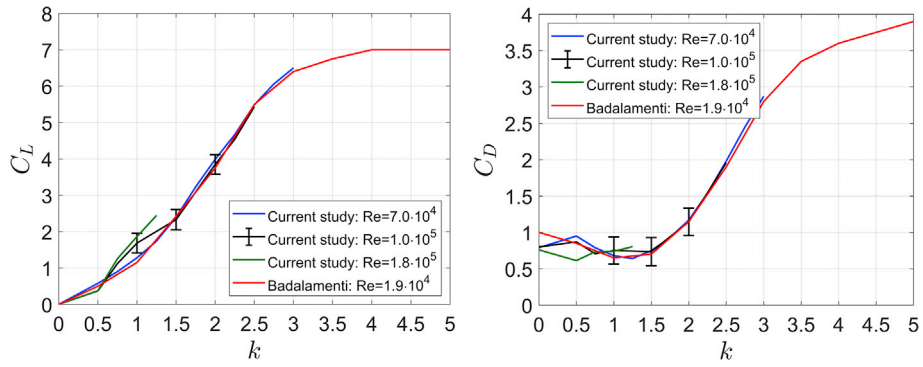

Fig. 9. Lift and drag coefficients of the single Flettner rotor compared with the results of (Badalamenti and Prince, 2008).

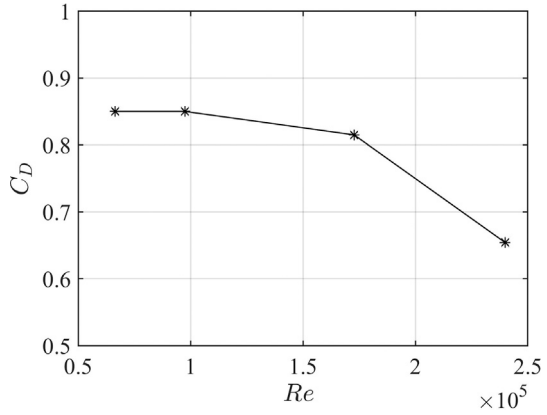

Fig. 10. Drag coefficient at increasing Reynolds numbers.

reduced and deviated due to the downwash caused by the Flettner rotor's circulation. At $k = 2$, the wake is fully suppressed and the flow is heavily deviated, up to an angle of about 40° at the distance $x/D = 1.5$. It should also be noted that, in general, the downwash is mainly appreciable in the range $-3 < y/D < 3$ and that, in the range $1 < y/D < 4$, the circulation causes the flow speed to increase compared to the free stream velocity. Higher velocity ratios mean a stronger circulation and, in turn, this leads to a more noticeable downwash and a more steep increase in wind speed in the range $1 < y/D < 4$. On the other hand, the circulation does not seem to cause any appreciable decrease in flow speed on the opposite side of the cylinder, in the range $-4 < y/D < -1$, where, in fact, the flow appears to have a speed comparable to the free stream velocity.

3.2. Results of two Flettner rotors

3.2.1. Lift and drag coefficients

The lift and drag coefficients of the two Flettner rotors were measured for several wind angles ranging between 15° and 180° (see conventions in Fig. 7) to investigate the influence of different relative positions with respect to the incoming wind on the cylinders' aerodynamic coefficients. Depending on the spacing, different wind angles were tested. These are reported in Table 1.

The reason why no experiments were conducted for spacing 15D and wind angle $WA = 90°$, is because, in this condition, the Flettner rotor positioned closer to the edge of the turntable would have been too near the wind-tunnel walls and this, arguably, would have jeopardized the measurements. Moreover, for the largest spacing, it was decided not to perform experiments at $WA = 45°$.

For each considered spacing and wind angle, the experiments on the two Flettner rotors comprised a matrix of nine tests generated by all combinations of velocity ratios $k = 1$, $k = 1.5$ and $k = 2$. During the experiments, in fact, one Flettner rotor spun at a given velocity ratio,

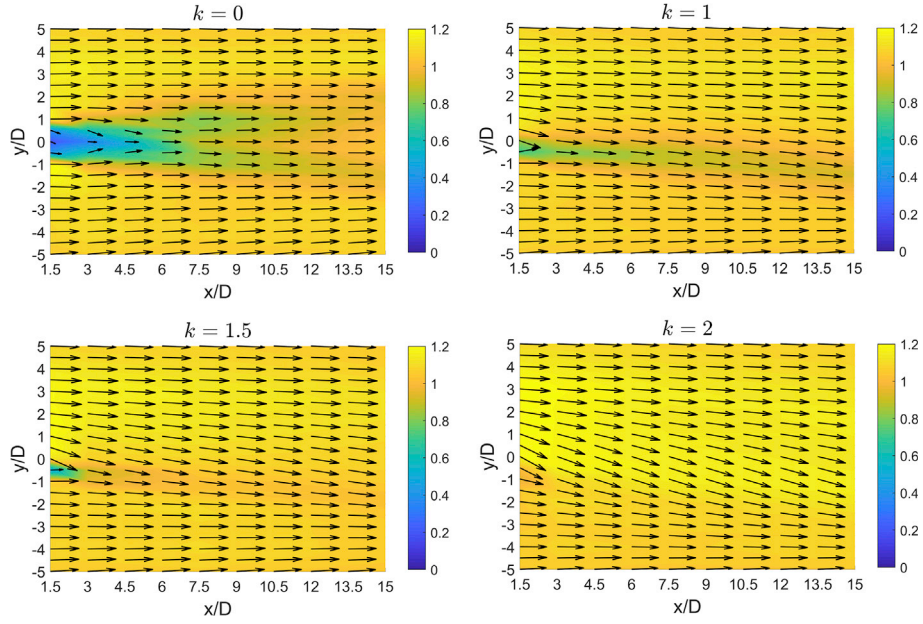

Fig. 11. Velocity field past the single Flettner rotor at different velocity ratios.

Table 1
Summary of the wind angles tested depending on the considered spacing.

Spacing	Wind angles [deg]							
3 *D*	15	30	45	60	90	120	150	180
7.5 *D*	15	30	45	60	90	120	150	180
15 *D*	15	30	–	60	–	120	150	180

while the other spun for the entire set of velocity ratios $k = 1$, $k = 1.5$ and $k = 2$. Lift and drag were measured for all velocity ratio combinations. The results reported in Fig. 12, Fig. 13 and Fig. 14 are also structured in this manner. In fact, the results for Flettner rotor A and Flettner rotor B show how, for the velocity ratio of interest, their lift and drag coefficients change due to the velocity ratio of the other Flettner rotor. The results of the single Flettner rotor used for the comparison are also reported for the same velocity ratio of interest. Following the conventions depicted in Fig. 7, when analyzing the results, it should be borne in mind that Flettner rotor A is windward with respect to Flettner rotor B until $WA = 90°$, whereas the opposite is true for wind angles $WA > 90°$.

The results given in Figs. 12, Figs. 13 and 14 show that the Flettner rotors' relative position has a considerable influence on how C_L and C_D are affected by the aerodynamic interaction. This is in agreement with the findings of the literature discussed in Section 1. It appears evident, in fact, that, generally, the effects of the Flettner rotors' aerodynamic interaction become less pronounced with the increase of the spacing. This holds true for any considered velocity ratio of interest. Moreover, the position of the two Flettner rotors with respect to the incoming wind direction, i.e. the wind angle, also appears to play an important role. When the two cylinders come close to being aligned with the incoming wind direction, in fact, C_L and C_D of the downstream Flettner rotor are strongly influenced by the interaction effects. This can be noticed looking at the results of Flettner rotor A for $150° \leq WA \leq 180°$ as well as those of Flettner rotor B for $15° \leq WA \leq 30°$. In these wind angle ranges, in fact, the downstream Flettner rotor is, at least partially, immersed in the wake generated by the upstream one and these are, generally, the regions where the most prominent variations of lift and drag coefficients occur. As suggested by the results of the velocity field measurements shown in Fig. 11, the variations of lift and drag coefficients are mainly caused by two phenomena: a change of the incoming flow velocity and a change in direction of the flow. The magnitude of these phenomena depends on the velocity ratio, that, therefore, is the key parameter that regulates how the

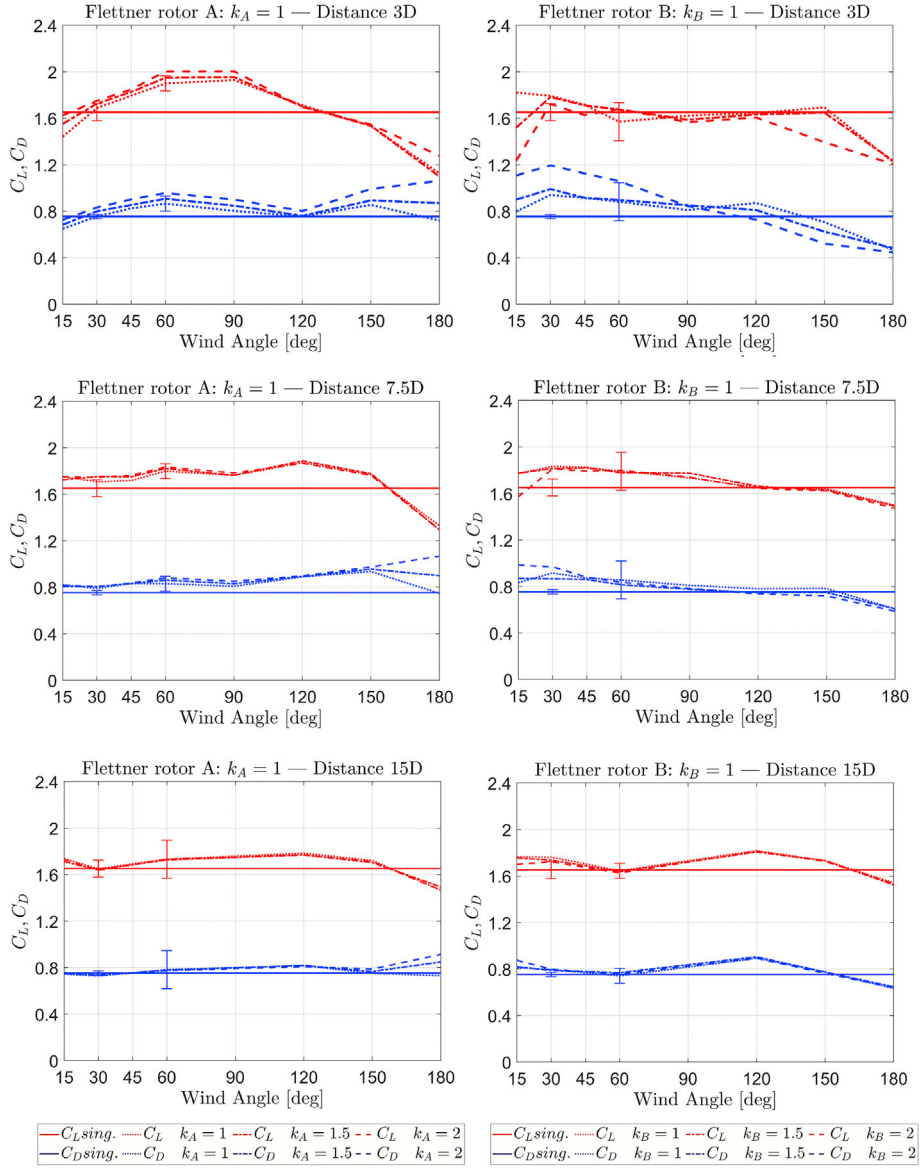

Fig. 12. Lift and drag coefficients for Flettner rotor A (left) and Flettner rotor B (right) for velocity ratio of interest $k = 1$.

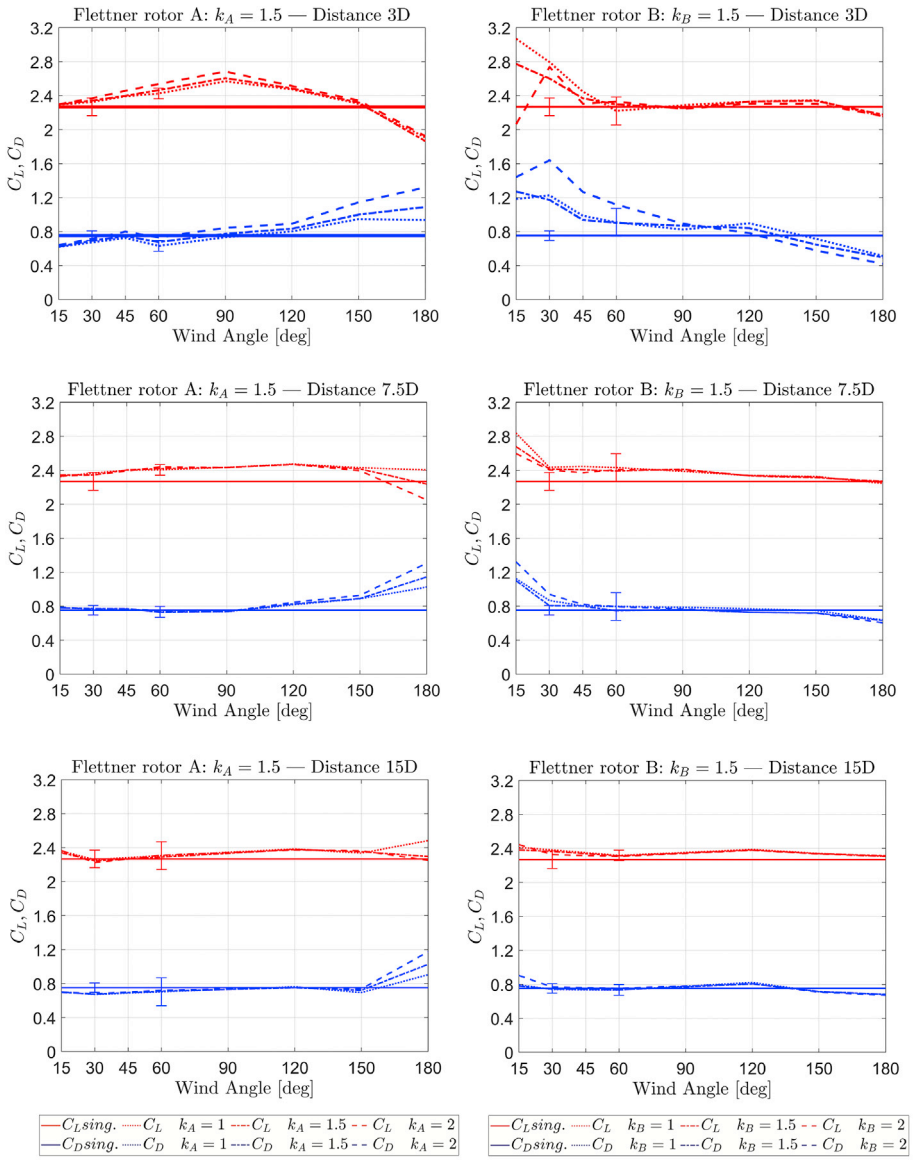

Fig. 13. Lift and drag coefficients for Flettner rotor A (left) and Flettner rotor B (right) for velocity ratio of interest $k = 1.5$.

aerodynamic interaction affects the Flettner rotor lift and drag coefficients. For example, when Flettner rotor A is in the wake of Flettner rotor B, i.e. $150° \leq WA \leq 180°$, its C_L decreases while its C_D increases. Although to a different extent, this is the case for all spacings considered (see Figs. 12, Figs. 13 and 14). The reason why this occurs is due to the change in direction of the flow, i.e. to the downwash caused by the circulation of the upstream Flettner rotor. As it can be noticed from the results, this trend becomes more pronounced with the increase of the velocity ratio of the upstream device (i.e. stronger circulation). Nonetheless, the trend here described is also influenced by the change in flow velocity. This is particularly the case for velocity ratios $k = 1$ and $k = 1.5$, for which a decrease of the flow velocity in the Flettner rotor's wake is still appreciable (Fig. 11). Differently from the change in the flow direction, the flow velocity reduction equally affects the lift and drag coefficients, namely, it decreases them to the same extent. Eventually, the lift and drag coefficients are affected by these two phenomena simultaneously. This can be observed in Fig. 12, for example, looking at the results of Flettner rotor A for $150° \leq WA \leq 180°$ and for the three considered spacings. At $WA = 180°$, when the velocity ratio of Flettner rotor B is $k = 1$, the drag coefficient of Flettner rotor A decreases with respect to $WA = 150°$. In fact, at $WA = 180°$ the two Flettner rotors are aligned with the wind direction and, in this condition, the flow velocity reduction appears to be a more prominent effect compared to the downwash. When the velocity ratio of Flettner rotor B is increased, however, this effect is no longer appreciable because at velocity ratios $k = 1.5$ and $k = 2$ the flow velocity reduction in the wake of Flettner rotor B is less impactful compared to the change in flow angle and, as previously explained, this leads to an increase of the drag coefficient.

Noticeable interaction effects do not only occur on the Flettner rotor that is the wake of the other, but they also occur when the Flettner rotors are in other relative positions. In the range $45° \leq WA \leq 120°$, in fact, the aerodynamic coefficients of Flettner rotor A appear to be considerably affected by the behaviour of Flettner rotor B. In Fig. 12, the drag coefficient and, more noticeably, the lift coefficient of Flettner rotor A are increased with respect to the corresponding coefficients of the single Flettner rotor. For $WA > 90°$, this is arguably due to the increase in flow speed caused by the circulation (of Flettner rotor B) as suggested by the results of the velocity field in Fig. 11 (see range $1 < y/D < 4$). This phenomenon becomes less pronounced with the increase of the spacing as well as with the increase of the velocity ratio of interest (see results of Flettner rotor A in Figs. 13 and 14). On the other hand, when Flettner rotor B is windward with respect to Flettner rotor A ($WA = 180°$), it

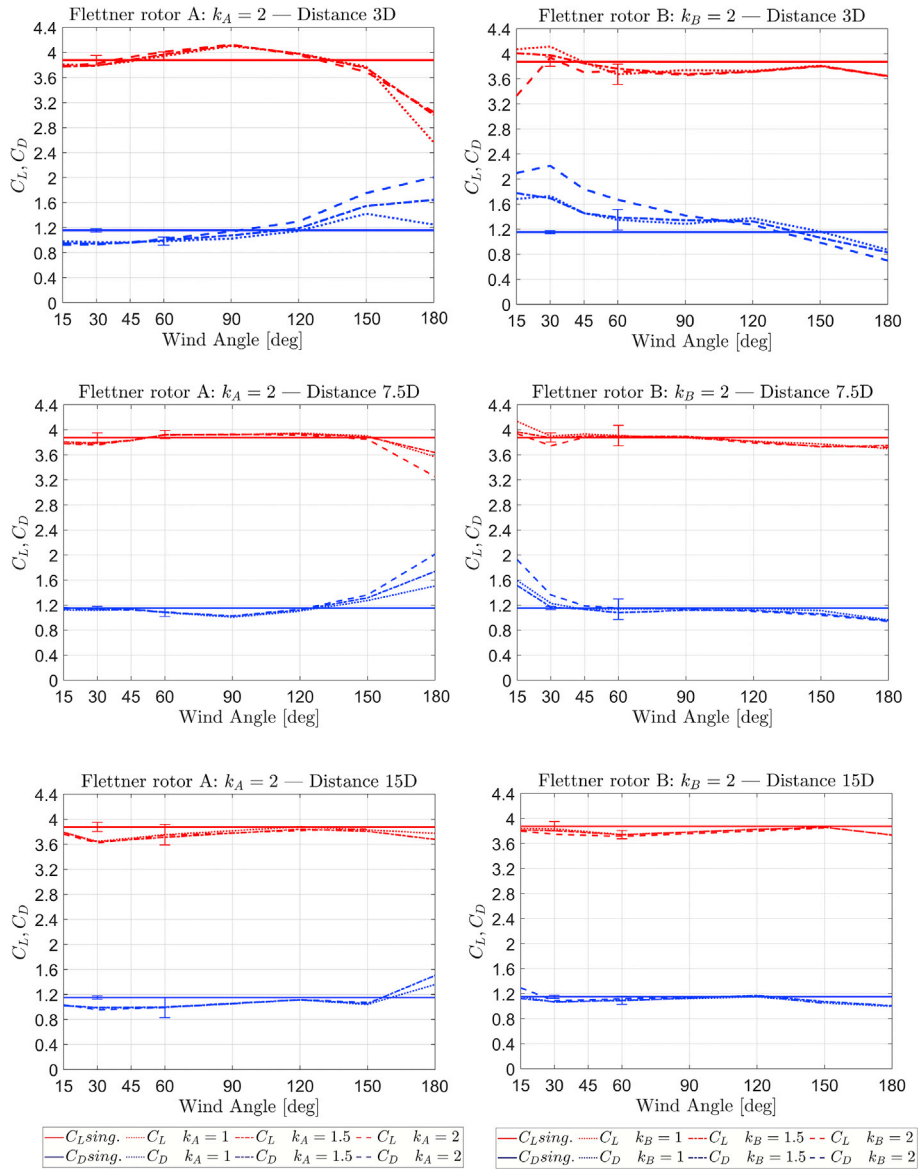

Fig. 14. Lift and drag coefficients for Flettner rotor A (left) and Flettner rotor B (right) for velocity ratio of interest $k = 2$.

appears to be influenced by the proximity of the latter. This effect is most prominent for the velocity ratio of interest $k = 1$ and for the shortest spacing (see results of Flettner rotor B in Fig. 12). Once again, this phenomenon becomes less evident with the increase of the spacing and, in general, also with the increase of the velocity ratio of interest (see results of Flettner rotor B in Figs. 13 and 14).

3.2.2. Driving and heeling force coefficients

As discussed in Section 3.2.1, the Flettner rotors' lift and drag coefficients depend on their velocity ratios as well as on their relative position with respect to the incoming wind direction. The driving and heeling force coefficients, on the other hand, are influenced by the Flettner rotors' velocity ratios, by their relative position with respect to the incoming wind direction but also by their layout on the ship's deck with respect to its heading. This means that, for one same spacing, the location where the Flettner rotors are installed on the ship's deck affect their resulting driving and heeling force coefficients. The Flettner rotors can be installed in any desired arrangement on the ship, however, in the current study, two arrangements that, arguably, are nowadays the most commonly used for real-life applications, are analysed. These are the tandem (Fig. 15) and the side-by-side arrangement (Fig. 16). An example

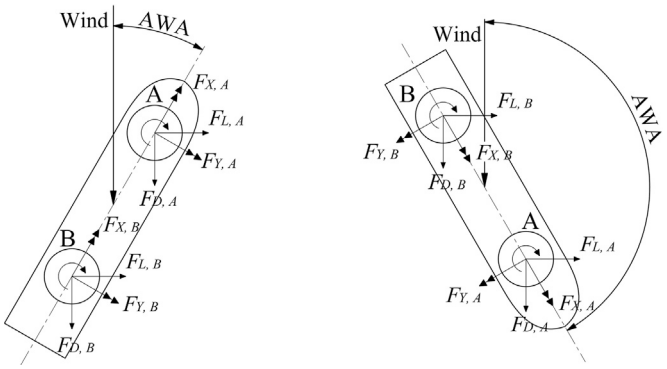

Fig. 15. Flettner rotors installed on the ship in tandem arrangement. Conventions for $AWA < 90°$ (left) and $AWA > 90°$ (right).

of a wind-assisted ship with two pairs of Flettner rotors installed, respectively, in side-by-side and tandem arrangement can be seen in Fig. 1.

The driving and heeling force coefficients are calculated from the lift

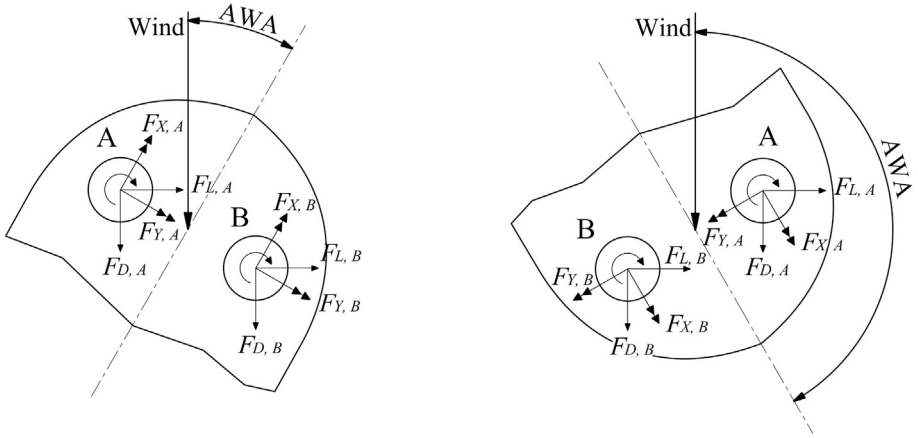

Fig. 16. Flettner rotors installed on the ship in side-by-side arrangement: conventions for $AWA < 90°$ (left) and $AWA > 90°$ (right).

and drag coefficients according to Eq. (4) and Eq. (5):

$$C_x = C_L \cdot sin(AWA) - C_D \cdot cos(AWA) \tag{4}$$

$$C_Y = C_L \cdot cos(AWA) + C_D \cdot sin(AWA) \tag{5}$$

where, in this context, the apparent wind angle AWA, is the angle between the incoming wind direction and the heading of the ship.

Due to the setup used during the experiments on the two Flettner rotors (see Fig. 7), the driving and heeling force coefficients were calculated for a different set of apparent wind angles depending on the type of arrangement considered. In particular, it occurs that the positions of the Flettner rotors depicted in Fig. 7 are analogous to the positions of the devices installed in tandem arrangement on the ship (Fig. 15). On the other hand, the positions of the Flettner rotors installed in side-by-side arrangement on the ship (Fig. 16) are rotated by 90° with respect to the setup used during the tests (Fig. 7). For example, given the conditions above described, the lift and drag results obtained at wind angle $WA = 30°$, were used to compute the driving and heeling force of the tandem arrangement for $AWA = 30°$, whereas for the side-by-side arrangement were used to calculate the results relative to $AWA = 120°$. In Table 2 the entire set of apparent wind angles analysed depending on the considered Flettner rotor arrangement are provided.

The present section aims at investigating the influence of the aerodynamic interaction on the performance of the considered Flettner rotor arrangements with respect to similar sets for which the interaction effects are neglected. To do so, the driving and heeling force coefficients are calculated according to Eq. (6) and Eq. (7) for the combination of the two Flettner rotors belonging to one same arrangement. These coefficients are then compared with those obtained for an analogous arrangement composed of two non-interacting devices whose data are derived from the results of the single Flettner rotor experiments.

$$C_X = (C_{X_A} + C_{X_B})/2 \tag{6}$$

$$C_Y = (C_{Y_A} + C_{Y_B})/2 \tag{7}$$

Considering the most common Flettner rotor installations currently in existence, the driving and heeling force coefficients when the two devices are in tandem arrangement are calculated for the three spacings tested during the experiments. Conversely, when the Flettner rotors are in side-by-side arrangement,C_X and C_Y are calculated only for the shortest spacing.

Figs. 17-20 show the results of the present analysis. Each case is investigated both in terms of C_X and C_Y coefficients and in terms of percentage change with respect to the case of two non-interacting Flettner rotors. For the sake of conciseness, for each spacing and arrangement type, only the most relevant results are reported herewith.

In Figs. 17 and 18 the results of the two Flettner rotors placed at a distance of three diameters are given. For this condition, the most noticeable finding is that the driving and heeling force coefficients largely differ depending on whether the devices are installed in tandem or side-by-side arrangement. In fact, when the two Flettner rotors are in tandem arrangement the most relevant interaction effects occur when the ship is sailing close hauled ($AWA = 30°$) or downwind ($AWA = 180°$). Conversely, for the side-by-side installation, the most evident interaction effects occur when the ship is sailing beam reach ($90° \leq AWA \leq 120°$). The magnitude of the interaction effects can be better appreciated by looking at the percentage change graphs reported at the bottom of the corresponding C_X and C_Y results.

Another substantial finding is that, for the same set of velocity ratios, the aerodynamic performance of the Flettner rotor ensemble varies depending on whether the windward Flettner rotor spins faster than the leeward one, or vice versa. This is evident, for example, for the side-by-side arrangement when the Flettner rotors spin at velocity ratios $k = 1$ and $k = 1.5$ and the apparent wind angle is $AWA = 105°$ (Fig. 18). In this condition, if the windward device (Flettner rotor A) spins at a higher velocity ratio than the leeward one (Flettner rotor B), the driving force coefficient of the Flettner rotor ensemble increases by nearly 20% with respect to the non-interacting Flettner rotors. On the other hand, this gain does not occur when Flettner B spins faster than Flettner rotor A.

With the exception of the largest spacing, and in particular for the tandem arrangement, the interaction effects occurring between the two Flettner rotors at apparent wind angles $AWA < 45°$ worsen the aerodynamic efficiency of the entire rig, i.e. C_X decreases and C_Y increases. This is due to the decrease in C_L and the increase in C_D of the leeward Flettner rotor due to the downwash generated by the windward device (see relative figures in Section 3.2.1). The same phenomenon, however, often has a positive effect on the overall performance of the rig when the apparent wind angle is $AWA = 180°$. This can be appreciated, for example, in Fig. 17 when both devices spin at velocity ratio $k = 2$ as well as in Fig. 19 for velocity ratios $k = 1.5$ and $k = 2$. In these conditions, in fact, the decrease in C_L and increase in C_D of the leeward Flettner rotor causes a rise of the driving force coefficient and a reduction of the heeling

Table 2
Apparent wind angles at which C_X and C_Y are calculated depending on the Flettner rotor arrangement.

Arrangement type	Apparent wind angles [deg]							
Tandem	30	45	60	90	120	150	180	–
Side by side	30	60	90	105	120	135	150	180

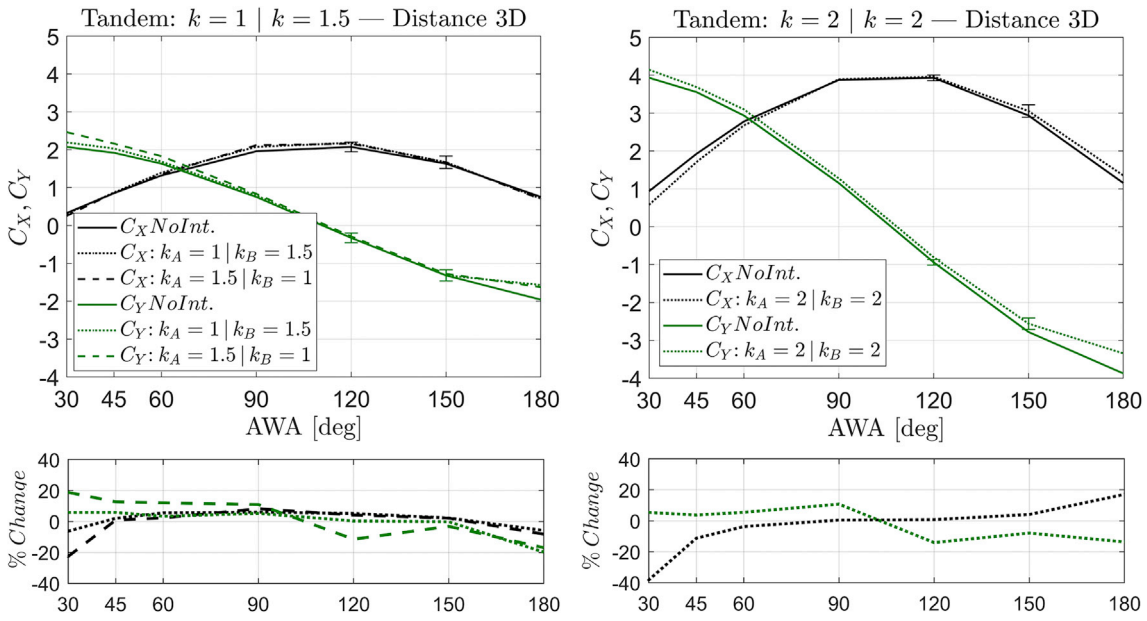

Fig. 17. Driving and heeling force coefficients (top) and their percentage change with respect to the non-interacting Flettner rotors (bottom), for two different sets of velocity ratios. Devices installed in tandem arrangement at a spacing of 3 diameters.

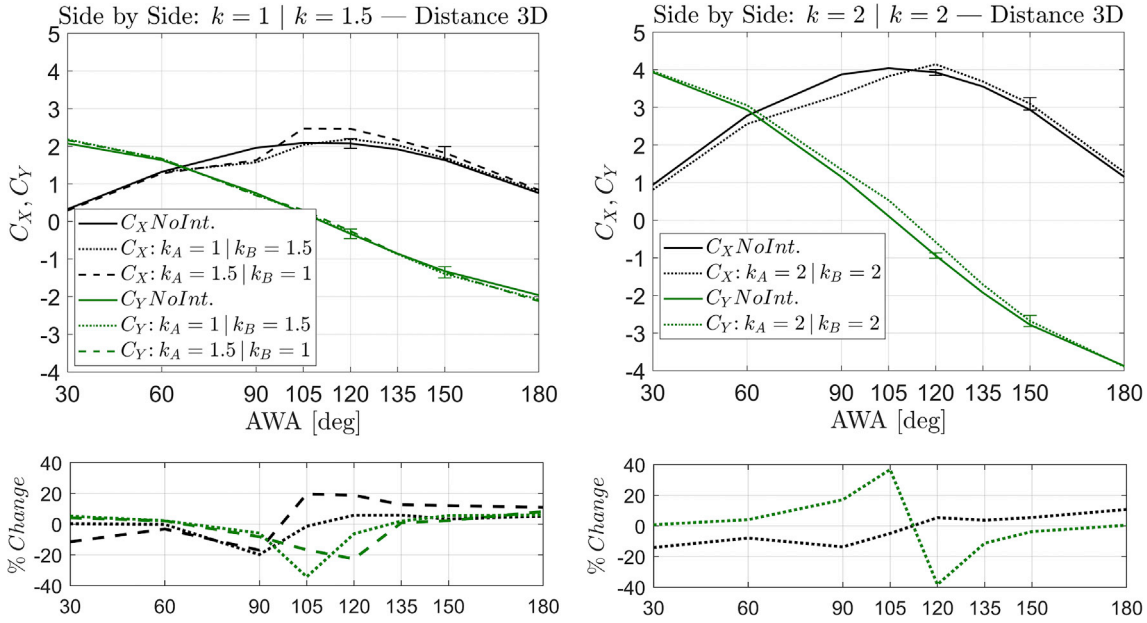

Fig. 18. Driving and heeling force coefficients (top) and their percentage change with respect to the non-interacting Flettner rotors (bottom), for two different sets of velocity ratios. Devices installed in side-by-side arrangement at a spacing of 3 diameters.

force coefficient of the Flettner rotor ensemble.

Following the trend of the results of the lift and drag coefficients, also for the driving and heeling force coefficients, the effects of the Flettner rotor aerodynamic interaction diminish with the increase of their spacing. When the Flettner rotors are set 15 diameters apart, the two devices operate more independently, and their aerodynamic coefficients become closer to those of two non-interacting Flettner rotors. The results given in Fig. 20, in fact, show that for apparent wind angles $60^\circ \leq AWA \leq 150^\circ$, the aerodynamic interaction has a minor influence on the driving and heeling force coefficients. Conversely, for $AWA < 60^\circ$ and $AWA > 150^\circ$, there is still a noticeable effect of the interaction on the aerodynamic performance of the considered Flettner rotors.

4. Influence of Reynolds number on the interaction effects

As demonstrated in Section 3.1, the experiments carried out at Reynolds number $Re = 1.0 \cdot 10^5$ were conducted in the subcritical flow regime. According to the results reported in the study of Bordogna et al. (2019), however, the Reynolds number influences the drag and, within certain conditions, the lift coefficient of a Flettner rotor. Arguably, it should be expected that this also plays a role in the way multiple Flettner rotors interact with each other. To investigate whether this is the case, during a previous experimental campaign conducted on a large-scale Flettner rotor (Bordogna et al., 2019), measurements of the velocity field were taken in the wake of the analysed rotating cylinder. The large-scale Flettner rotor had a diameter $D = 1.0$ m and a span $H = 3.73$

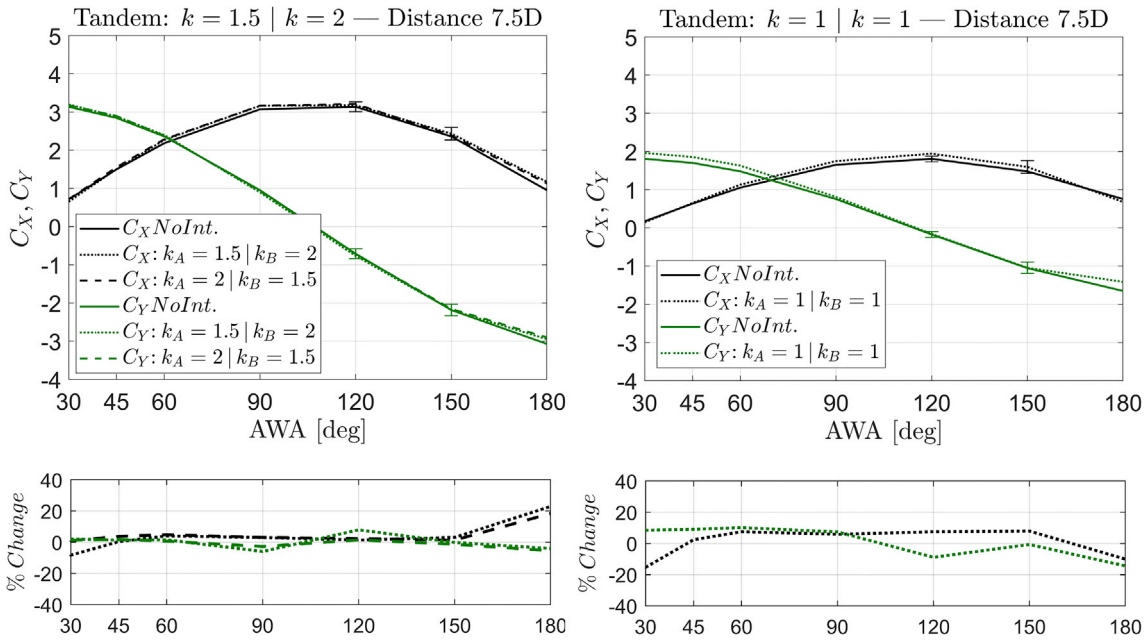

Fig. 19. Driving and heeling force coefficients (top) and their percentage change with respect to the non-interacting Flettner rotors (bottom), for two different sets of velocity ratios. Devices installed in tandem arrangement at a spacing of 7.5 diameters.

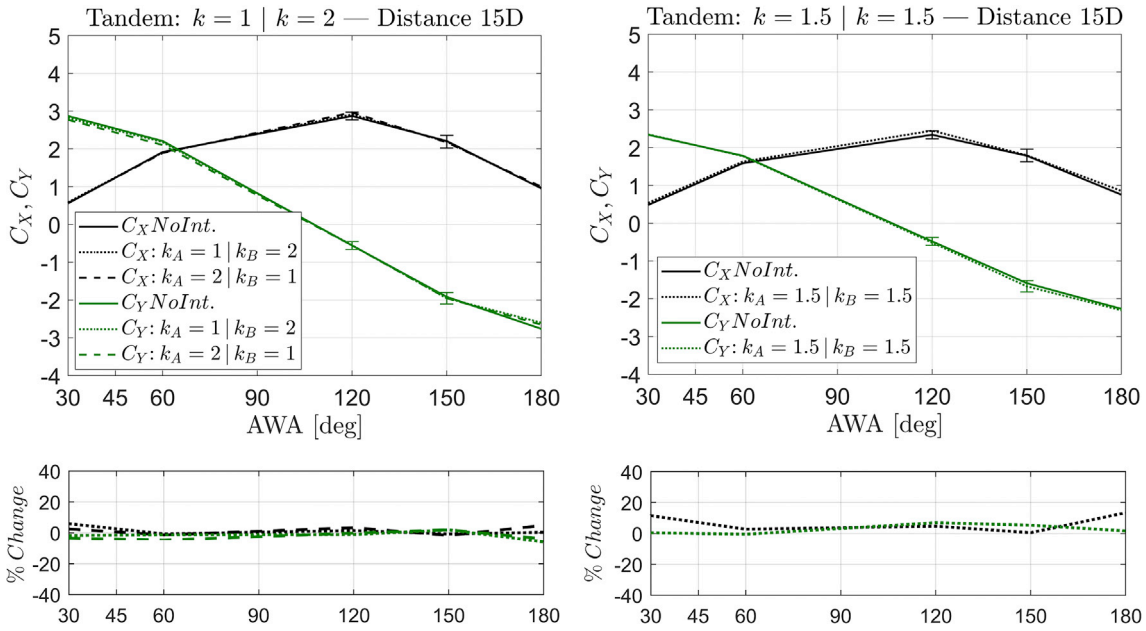

Fig. 20. Driving and heeling force coefficients (top) and their percentage change with respect to the non-interacting Flettner rotors (bottom), for two different sets of velocity ratios. Devices installed in tandem arrangement at a spacing of 15 diameters.

m. Due to its span and considering that the experiments took place in the same test section described in Section 2.1, the tip vortices were suppressed and, in this sense, the tests can be deemed two-dimensional. See the publication of Bordogna et al. (2019) for further details. The velocity field was measured using the same type of equipment described in Section 2.3, however, in this case, being the flow two-dimensional, measurements were only taken at the Flettner rotor mid-span height. Tests were carried out for two Reynolds number, namely $Re = 2.5 \cdot 10^5$ (critical regime) and $Re = 5.5 \cdot 10^5$ (supercritical regime), and for three different velocity ratios, i.e. $k = 1$, $k = 2$ and $k = 3$. Following the same conventions used in Fig. 11, the results of the velocity field measurements are reported in terms of mean velocity magnitude and mean direction of the flow. The velocity magnitude, that is normalized with the free stream velocity, is indicated by the colourmap and the vector size. On the other hand, the direction of the flow is suggested by the vector orientation. Also for the results reported in Fig. 21 it should be assumed that the Flettner rotor is located at the centre of the reference system ($x/D = 0, y/D = 0$) and it rotates clockwise. It should be pointed out, however, that due to the major dimensions of the large-scale Flettner rotor, a reduced number of positions in terms of x/D and y/D were tested compared to the experiments carried out on the smaller Flettner rotor used in the present work (see Figs. 11 and 21).

The results reported in Fig. 21 show a trend comparable to the results depicted in Fig. 11. In fact, it can be appreciated that the increase of the

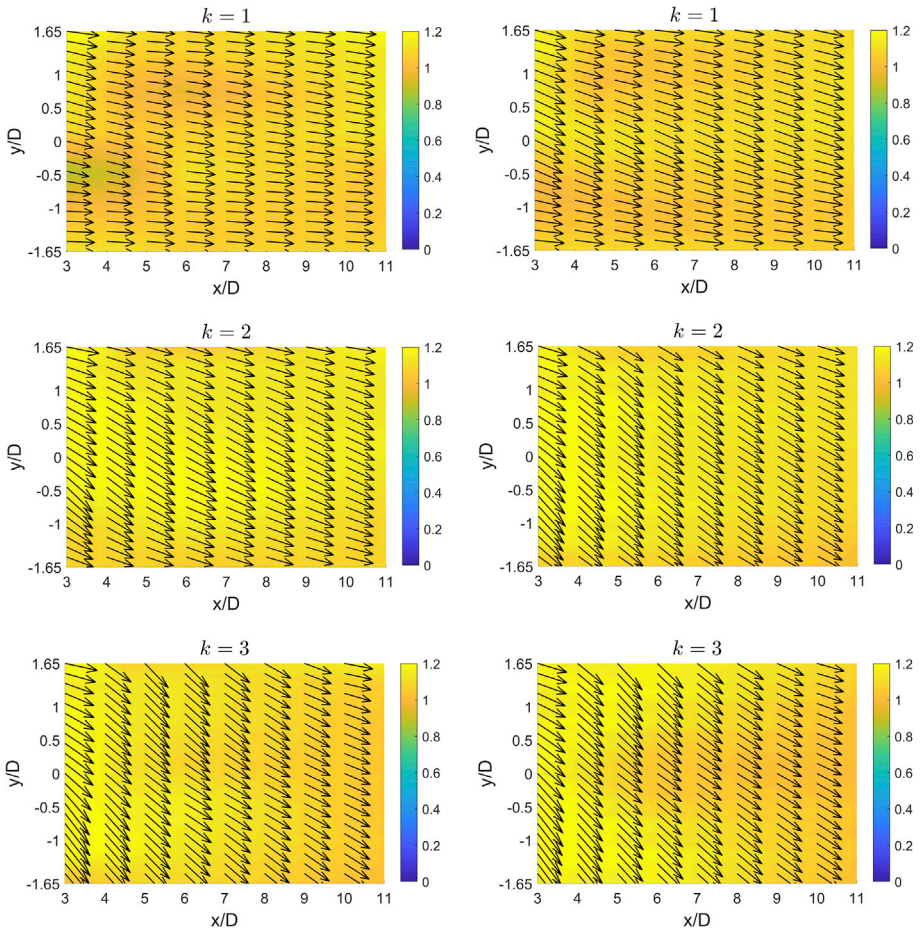

Fig. 21. Velocity field past the large-scale Flettner rotor for different velocity ratios: $Re = 2.5 \cdot 10^5$ (left) and $Re = 5.5 \cdot 10^5$ (right).

velocity ratio reduces the velocity deficit in the wake of the Flettner rotor while it intensifies the deflection of the flow. The Reynolds number appears to have a similar effect. At velocity ratio $k = 1$, in fact, an area of reduced velocity can be found at $y/D = -0.5$ and $3 \leq y/D \leq 4$ for $Re = 2.5 \cdot 10^5$. At Reynolds number $Re = 5.5 \cdot 10^5$, however, this is no longer visible. Also, at the higher Reynolds number, the flow appears to be more deflected. This is the case both for $k = 1$ and for $k = 2$, while for $k = 3$ this does not occur. A plausible explanation of this phenomenon can be found by looking at the results of the influence of the Reynolds number on the Flettner rotor lift coefficient (see Fig. 22).

As discussed in Section 3.1, in fact, the circulation in the flow caused by the Flettner rotor spin alters the velocity field: the circulation tends to deflect the direction of the flow and to suppress the velocity deficit in the Flettner rotor's wake. Since lift is directly dependent on circulation, looking at Fig. 22, it can be appreciated the reason why a higher Reynolds number causes a larger flow deflection and a more noticeable suppression of the velocity deficit in the Flettner rotor's wake. It appears, in fact, that a higher Reynolds number entails a higher lift coefficient. Nonetheless, this is the case up to velocity ratio $k = 2.5$, above which the Reynolds number influence seems to be negligible. This is reflected in the results of the velocity field measurements depicted in Fig. 21. For velocity ratio $k = 3$, in fact, no significant differences can be noticed for the results obtained at $Re = 2.5 \cdot 10^5$ and at $Re = 5.5 \cdot 10^5$. Moreover, Fig. 22 also indicates that above $Re = 3.6 \cdot 10^5$ the lift coefficient seems to be insensitive to scale effects. Using the same rationale, therefore, it could be assumed that above this threshold the Reynolds number does not influence the velocity field past a Flettner rotor. In turn, it can be argued that, in the supercritical flow regime, the Reynolds number does not affect the aerodynamic interaction occurring between multiple Flettner rotors.

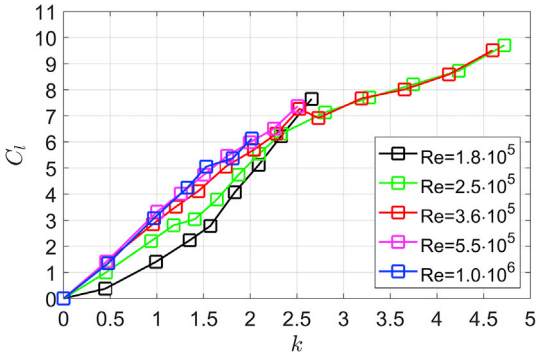

Fig. 22. Lift coefficient of the large-scale Flettner rotor at different Reynolds numbers as reported by Bordogna et al. (2019).

5. Conclusions

The present investigation deals with a series of wind-tunnel experiments on two similar Flettner rotors aimed at gaining more insight regarding the effects of the aerodynamic interaction on their performance. To provide a baseline for comparison, previous tests were carried out on a single Flettner rotor for analogous conditions. The results of the experimental campaign are reported in terms of lift and drag coefficients, as well as in the form of driving and heeling force coefficients. In the former case, the effects of the aerodynamic interaction occurring between the two Flettner rotors are shown on the lift and drag coefficients

of each device. From the results, it is understood that the velocity ratio of each Flettner rotor and their relative position (spacing and wind angle) are determining factors for the influence of the aerodynamic interaction on the Flettner rotor performance. In particular, it is shown that the interaction effects are, generally, most noticeable for shorter spacings and when the two Flettner rotors come close to being aligned with the wind direction. The role of the velocity ratio appears to be more complex but, nonetheless, distinguishable trends can be identified with the aid of the velocity field measurements carried out in the wake of the single Flettner rotor. From these results, two main phenomena could be detected: the change of the incoming wind speed and the deflection of the incoming flow angle. For the former, a decrease of the incoming wind speed is found at lower velocity ratios whereas higher k values lead to an increase of the wind speed with respect to the freestream velocity. For the latter, it is understood that the downwash gains strength with the increment of the velocity ratio. For most cases, sensible conclusions can be drawn by applying the findings of the velocity field measurements to the results of the lift and drag coefficients. The driving and heeling force coefficients are presented for the combination of the two Flettner rotors and compared for similar sets of two non-interacting devices. The output of C_X and C_Y is the consequence of the trends of the lift and drag coefficients. In this case, however, it is demonstrated that the Flettner rotor layout on the ship's deck (in the current study, tandem versus side-by-side arrangement) is a key factor for the aerodynamic performance of the entire rig. Depending on the type of arrangement, the control of the velocity ratio of each Flettner rotor, i.e. whether the windward device rotates faster or slower than the leeward one, has the capacity to mitigate the detrimental effect of the aerodynamic interaction or, in some cases, to increase the performance of the entire rig with respect to a comparable set of non-interacting devices. In general, it can be concluded that the best overall aerodynamic performance (that does not necessarily coincide with the best performance of the ship due to the coupling between its aero/hydrodynamic forces) is reached when the Flettner rotors are set furthest apart, i.e. when their aerodynamic interaction is minimized. In case this condition is not achievable due, for example, to a limited deck space, it is shown that for the shortest spacing a higher aerodynamic efficiency is attained when the Flettner rotors are set in side-by-side arrangement for $AWA < 60°$, and, for $AWA > 60°$, when the devices are installed in a tandem arrangement. Finally, it is argued that the Reynolds number may affect the aerodynamic interaction occurring between multiple Flettner rotors. For the conditions analysed, it appears that scale effects may become marginal for velocity ratios $k \geq 2.5$ and when the flow is in a supercritical regime. Further research should be conducted on this topic to investigate the veridicality of these assumptions.

Acknowledgements

This research is part of the Sail Assist project and it is supported by the Sea Axe Fund and the Vaderlandsch Fonds. The author would like to thank the research sponsors as well as all the staff at Politecnico di Milano wind tunnel for their kind help.

References

Assi, G.R.S., Bearman, P.W., Meneghini, J.R., 2010. On the wake-induced vibration of tandem circular cylinders: the vortex interaction excitation mechanism. J. Fluid Mech. 661, 365–401.
Badalamenti, C., Prince, S.A., 2008. The effects of endplates on a rotating cylinder in crossflow. In: Proceedings of the 26th AIAA Applied Aerodynamics Conference, Honolulu, USA.
Badalamenti, C., 2010. On the Application of Rotating Cylinders to Micro Air Vehicles. Doctoral Thesis, City University, London.
Belloli, M., Muggiasca, S., Rosa, L., Zasso, A., 2016. Experimental study on the aerodynamic behaviour of a circular cylinder with perforated shrouding. In: Proceedings of the 8th International Colloquium on Bluff Body Aerodynamics and Applications, Boston, USA.
Bearman, P.W., 2011. Circular cylinder wakes and vortex-induced vibrations. J. Fluids Struct. 27, 648–658.
Bordogna, G., Muggiasca, S., Giappino, S., Belloli, M., Keuning, J.A., Huijsmans, R.H.M., van 't Veer, A.P., 2019. Experiments on a Flettner rotor at critical and supercritical Reynolds numbers. J. Wind Eng. Ind. Aerodyn. 188, 19–29.
De Marco, A., Mancini, S., Pensa, C., Calise, G., De Luca, F., 2016. Flettner rotor concept for marine applications: a systematic study. Int. J. Rotating Mach. 2016, 12. Article ID 3458750.
Diana, G., Belloli, M., Giappino, S., Manenti, A., Mazzola, L., Muggiasca, S., Zuin, A., 2014. Wind tunnel tests on two cylinders to measure subspan oscillation aerodynamic forces. Proc. IEEE Trans. Power Deliv. 29 (No. 3).
Eggers, R., 2016. Operational performance of wind assisted ships. In: Proceedings of the 10th Symposium on High-Performance Marine Vehicles, Cortona, Italy.
ESDU, 2012. Cylinder Groups: Mean Forces on Pairs of Long Circular Cylinders. ESDU 84015, London, UK.
Fallah, K., Fardad, A., Sedaghatizadeh, N., Fattahi, E., Ghaderi, A., 2011. Numerical simulation of flow around two rotating circular cylinders in staggered arrangement by multi-relaxation-time lattice Boltzmann method at low Reynolds numbers. World Appl. Sci. J. 15, 544–554.
Flettner, A., 1925. The Flettner Rotorship. Eng. 19, 117–120.
Garzon, F., Figueroa, A., 2017. The study on the flow generated by an array of four Flettner rotors: theory and experiment. Appl. Math. 8, 1851–1858.
Guo, X., Lin, J., Tu, C., Wang, H., 2009. Flow past two rotating circular cylinders in a side-by-side arrangement. J. Hydrodyn. 21, 143–151.
ISO/IEC 98-3, 2008. Guide to the Expression of Uncertainty in Measurement (GUM). International Organization for Standardisation, Geneva, Switzerland.
Kumar, S., Gonzalez, B., Probst, O., 2011. Flow past two rotating cylinders. Phys. Fluids 23, 014102 (2011).
Li, D.Q., Leer-Andersen, M., Allenström, B., 2012. Performance and vortex formation of Flettner rotors at high Reynolds numbers. In: Proceedings of the 29th Symposium on Naval Hydrodynamics, Gothenburg, Sweden.
Pearson, D., 2014. The use of Flettner rotors in efficient ship design. In: Proceedings of the Influence of EEDI on Ship Design Conference, London, UK.
Prandtl, L., 1926. Application of the Magnus Effect to the Wind Propulsion of Ships. NACA TM-367, Washington, USA.
Sumner, D., 2010. Two circular cylinders in cross-flow: a review. J. Fluids Struct. 26, 849–899.
Sungnul, S., Moshkin, N.P., 2009. Effect of rotation rates and gap spacing on the structure of low Reynolds number flow over two rotating circular cylinders. Computational Fluid Dynamics 2008. Springer, Berlin, Heidelberg.
Traut, M., Bows, A., Gilbert, P., Mander, S., Stansby, P., Walsh, C., Wood, R., 2012. Low C for the high seas: Flettner rotor power contribution on a route Brazil to UK. In: Proceedings of the Low Carbon Shipping Conference, Newcastle, UK.
Traut, M., Gilbert, P., Walsh, C., Bows, A., Filippone, A., Stansby, P., Wood, R., 2014. Propulsive power contribution of a kite and a Flettner rotor on selected shipping routes. Appl. Energy 13, 362–372.
Ueda, Y., Sellier, A., Kida, T., Nakanishi, M., 2003. On the low-Reynolds-number flow about two rotating circular cylinders. J. Fluid Mech. 495, 255–281.
Watson, E.J., 1995. The rotation of two circular cylinders in a viscous fluid. Mathematika 42, 105–126.
Yoon, H.S., Chun, H.H., Kim, J.H., Park, I.L.R., 2009. Flow characteristics of two rotating side-by-side circular cylinder. Comput. Fluids 38, 466–474.
Zdravkovich, M.M., 2003. Flow Around Circular Cylinders - Vol 2: Applications. Oxford University Press, New York.